Tectonophysics 913 (2025) 230875

Contents lists available at ScienceDirect

Tectonophysics

journal homepage: www.elsevier.com/locate/tecto

Along-strike variations in intermediate-depth seismicity in the southernmost Mariana subduction zone: Impact from the subduction of an oceanic plateau

Han Chen [a,b], Gaohua Zhu [c,*], Hongfeng Yang [b,d,**], Jiangyang Zhang [e], Shaopin Lu [a], Chuanxu Chen [f], Jian Lin [g,h], Yiming Luo [g,h]

[a] School of Earth Sciences and Engineering, Sun Yat-sen University & Southern Marine Science and Engineering Guangdong Laboratory (Zhuhai), Zhuhai, Guangdong, China
[b] Department of Earth and Environmental Science, Faculty of Science, The Chinese University of Hong Kong, Shatin, Hong Kong, China
[c] Key Laboratory of Ocean Observation and Forecasting, Institute of Oceanology, Chinese Academy of Sciences, Qingdao, China
[d] Shenzhen Research Institute, The Chinese University of Hong Kong, Shenzhen, China
[e] South China Sea Institute of Oceanology, Chinese Academy of Sciences, Guangzhou, China
[f] Institute of Deep-sea Science and Technology, Chinese Academy of Sciences, Sanya, China
[g] Department of Ocean Science and Engineering, Southern University of Science and Technology, Shenzhen, China
[h] Advanced Institute for Ocean Research, Southern University of Science and Technology, Shenzhen, China

ARTICLE INFO

Keywords:
Intermediate-depth earthquakes
Ocean Bottom Seismometer
Mariana subduction zone
EQTransformer
Subduction of oceanic plateau

ABSTRACT

Intermediate-depth earthquakes, i.e., earthquakes occurring at depths of 60 to 300 km, have been observed globally. However, the mechanisms underlying intermediate-depth earthquakes and their potential relationship with shallow subduction zone structures are still poorly understood. Utilizing newly obtained near-field Ocean Bottom Seismometer (OBS) data and a machine-learning-based method (EQTransformer), we have detected and located 613 earthquakes from 5 September 2018 to 22 October 2019. The observation identifies the variations in the distribution patterns of intermediate-depth earthquakes at the junction of the Pacific plate and the Caroline Plateau. Double seismic zones (DSZs) were observed in the Pacific segment, while a single seismic zone (SSZ) was found in the Caroline segment. The consistency between observed seismicity patterns, tectonic geomorphology, outer-rise faulting, and slab P-T modeling strongly suggests intermediate-depth earthquakes are likely related to the dehydration of hydrous minerals. We propose that the seismicity difference between the two segments is attributed to the subducted oceanic plateau, which restricts hydration of the subducting plate thereby suppressing the generation of intermediate-depth earthquakes. Our results emphasize the important influence of oceanic plateau subduction in the generation and distribution of intermediate-depth earthquakes.

1. Introduction

Intermediate-depth earthquakes are intraplate earthquakes within the subducted plates with depths of around 60 to 300 km (Gutenberg and Richter, 1954). Investigations of intermediate-depth earthquakes have enhanced knowledge of the Earth's structure, subduction process, and plate tectonics theory (Aki and Lee, 1976; Christova and Scholz, 2003; Hirahara, 1977; Isacks et al., 1968; Owens et al., 1984; Revenaugh and Jordan, 1991). Intermediate-depth earthquakes differ from shallow events in their seismogenic mechanisms, as the high pressure and temperature at these depths promote ductile rather than brittle deformation (Frohlich, 2006). Several mechanisms have been proposed to explain intermediate-depth earthquakes (Zhan, 2020), including transformational faulting (Incel et al., 2017; Kao and Liu, 1995), self-localizing thermal shear runaway (Kelemen and Hirth, 2007; Ogawa, 1987; Prakash et al., 2023; Prieto et al., 2013; Wiens and Snider, 2001), dehydration embrittlement (Green and Houston, 1995; Kirby, 1995; Mark et al., 2024; Pérez-Forero et al., 2023), fluid-related embrittlement (van Keken et al., 2012; Wei et al., 2017), dehydration-driven stress transfer (Ferrand et al., 2017) and inner slab stress and strain changes

* Corresponding author at: Key Laboratory of Ocean Observation and Forecasting, Institute of Oceanology, Chinese Academy of Sciences, Qingdao, China.
** Corresponding author at: Department of Earth and Environmental Science, Faculty of Science, The Chinese University of Hong Kong, Shatin, Hong Kong, China.
E-mail addresses: zhugaohua@qdio.ac.cn (G. Zhu), hyang@cuhk.edu.hk (H. Yang).

https://doi.org/10.1016/j.tecto.2025.230875
Received 12 November 2024; Received in revised form 2 August 2025; Accepted 4 August 2025
Available online 5 August 2025

(Malatesta et al., 2024; Zeng et al., 2025). However, there is still controversy among these views, and the mechanism of intermediate-depth earthquakes is not yet clear.

The spatial pattern of intermediate-depth earthquakes—occurring in either single seismic zones (SSZs) or double seismic zones (DSZs) subparallel along the subducted slab—may provide critical insights into this question. The DSZs have been observed globally in subduction zones (Fig. 1) (Brudzinski et al., 2007; Florez and Prieto, 2019; Sippl et al., 2022; Wiens et al., 1993), with the separation distance between the two seismicity layers ranging from 10 km to 40 km (Brudzinski et al., 2007; Frohlich, 2006). While the global ubiquity of SSZs remains unresolved, their existence has been documented in several subduction zones, such as the Aleutian, Kyushu, and Tonga, Izu Bonin, and Hikurangi trenches (Hudnut and Taber, 1987; Wei et al., 2021; Wei et al., 2017). The formation of DSZs was initially attributed to the unbending of the subducted plate, with downdip compressional earthquakes occurring in the upper seismogenic layer and extensional earthquakes in the lower layer (Engdahl and Scholz, 1977; Wang, 2002). However, observations revealed downdip extensional events in the upper layer (Dorbath et al., 2008; Kao and Rau, 1999; McGinty et al., 2000; Ratchkovsky et al., 1997; Sippl et al., 2019), suggesting other mechanisms have played a role.

Studies have linked along-strike variations in intermediate-depth earthquake distribution to features of subducting plate, including the outer-rise fault (Boneh et al., 2019; Kirby et al., 1996a; Ranero et al., 2003), topographic changes (Geersen et al., 2022; Nakajima, 2019), orientation of pre-existing fabrics, and subducted sediment thickness (Wei et al., 2021). The observed correlation between seismic distribution and plate features is suggested to result from variations in hydration-dehydration conditions (Boneh et al., 2019; Geersen et al., 2022; Nakajima, 2019; Wei et al., 2021). In particular, the transition between SSZ and DSZs has been observed in several subduction zones, such as the Aleutian, Kyushu, and southern Tonga trenches. The spatial patterns of intermediate-depth earthquakes reflect multiple controlling factors of intermediate-depth earthquake genesis, such as slab stress state and thermal structure (Hudnut and Taber, 1987; Wei et al., 2017), regional tectonic structure and slab ages (Nakajima, 2019), as well as pre-existing fabrics, and sediments on the slab (Wei et al., 2021). Therefore, investigating the transition of intermediate-depth earthquakes in layered structures might provide insights into their seismogenic mechanisms.

The southernmost segments of the Mariana subduction zone, where the young North Caroline Plateau is subducting along with the old Pacific plate (Fig. 2), provide a natural laboratory for investigating both

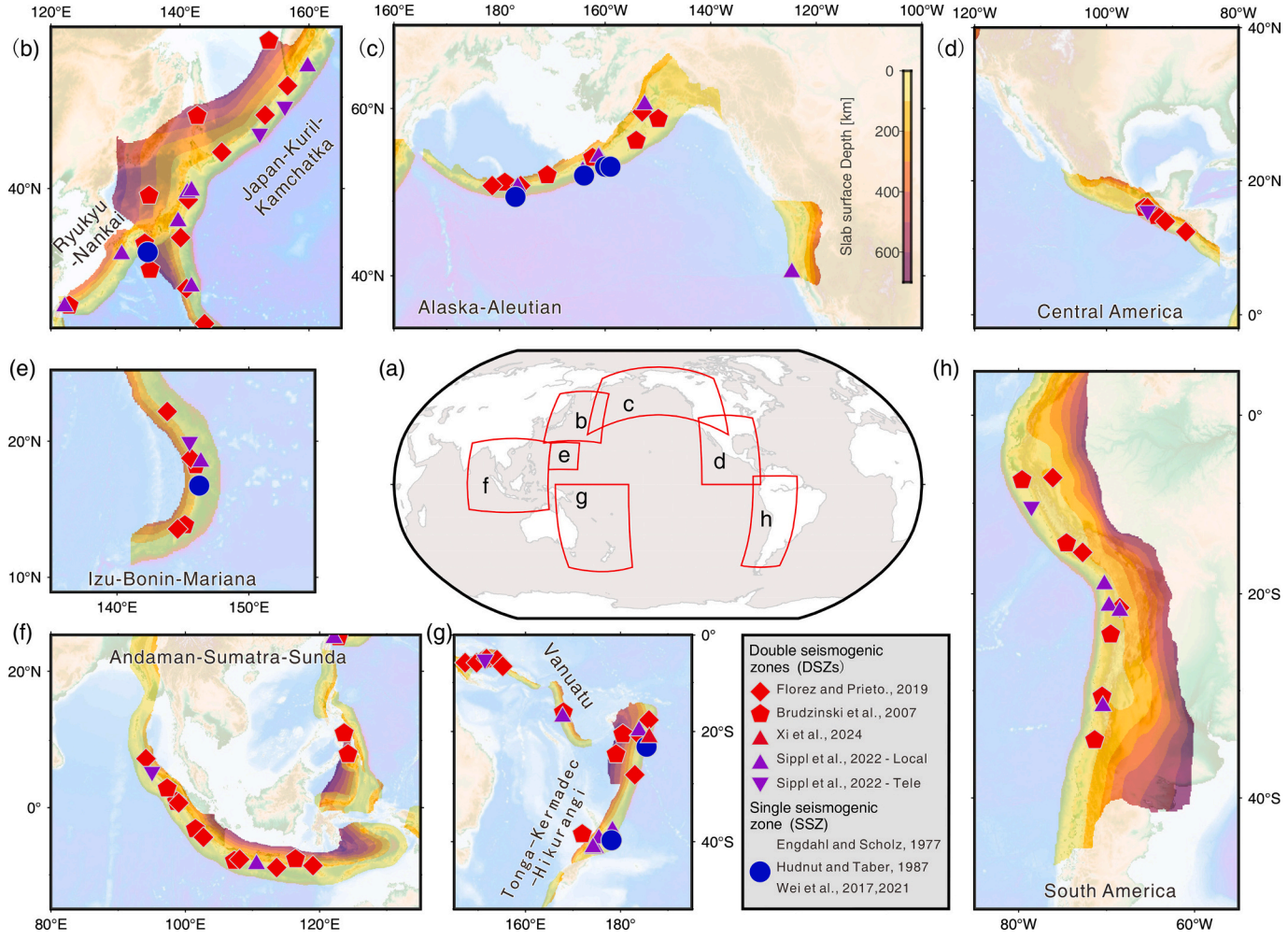

Fig. 1. Map of intermediate-depth earthquakes in subduction zones globally, the slab surface depth is from slab 2.0 data (Hayes, 2018). (a) Global map view of locations of panels b-h. (b) Japan-Kuril-Kamchatka subduction zones. (c) Aleutian-Cascadia and Mexican subduction zones. (d) Central American margin. (e) Mariana subduction zone. (f) Andaman-Sumatra-Java margin. (g) Tonga subduction zones. (h) South American margin. The locations of observed DSZs (red pentagons, red rhombus, purple triangles, green inverted triangles) come from (Sippl et al., 2022; Xi et al., 2024). The SSZ (blue circles) come from (Engdahl and Scholz, 1977; Hudnut and Taber, 1987; Nakajima, 2019; Wei et al., 2021; Wei et al., 2017). The data points shown in the figure are not exhaustive. (For interpretation of the references to colour in this figure legend, the reader is referred to the web version of this article.)

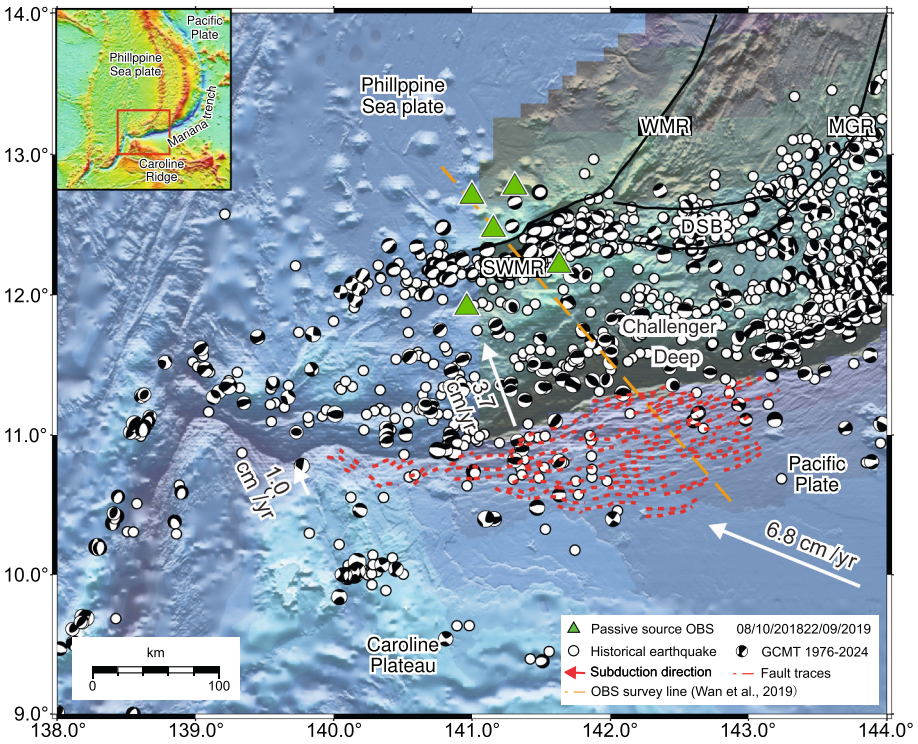

Fig. 2. Map of the OBS network and tectonic setting in the southernmost Mariana subduction zone. Green triangles indicate the locations of OBS. The shaded area shows the subducted slab from slab 2.0 model *(*Hayes, 2018*)*. The red dashed lines represent the major faults in the outer-rise regions. The dashed orange line represents the active air-gun source OBS profile *(*Wan et al., 2019*)*. The white arrows indicate the subduction rate of the slab *(*Kotake, 2000*;* Lee, 2004*;* Schellart, 2023*)*. White circles and beach balls represent the earthquake catalog from International Seismological Centre (ISC, 1962–2024) and Global Centroid Moment Tensor Project (GCMT, 1976–2024), respectively. SWMR, Southwest Mariana rift; WMR, West Mariana Ridge; MGR, Malaguana-Gadao Ridges; DSB, Diffuse spreading belt. (For interpretation of the references to colour in this figure legend, the reader is referred to the web version of this article.)

the transition of intermediate-depth earthquakes layered structure and subducting plate influences. Several previous studies have shown a highly hydrated subducting plate in the Pacific segment, evidenced by the deep-cutting outer-rise fault and seismicity (Chen et al., 2022; Emry et al., 2014; Zhou and Lin, 2018; Zhu et al., 2019) and reduction of seismic velocities (He et al., 2025; Wan et al., 2019; Zhu et al., 2021). On the other hand, most studies about the Caroline Ridge subduction focus on the subduction in the Yap Trench (Altis, 1999; Fan et al., 2022; Sangana et al., 2022; Zhang et al., 2021; Zhu et al., 2024), the segment in the southernmost Mariana subduction zone has received less attention. Previous near-field earthquake catalogs derived from ocean bottom seismometer (OBS) arrays deployed near the Pacific plate segment (Chen et al., 2022; Zhu et al., 2019) exhibited limited resolution for the Caroline segment, introducing a regional bias (Fig. 3).

In this study, we utilized a one-year deployment of OBS in the southern Mariana back-arc region simultaneously monitoring intermediate-depth seismicity across both the Pacific and Caroline segments, to investigate the characteristics of intermediate-depth earthquakes and the subducting plate influences. Earthquakes were detected using a machine-learning phase picker, and then located and magnitude-calibrated. The slab thermal structures in both segments were modeled, and the seismogenic mechanism was analyzed. Our observations revealed DSZs and SSZ in the subducted Pacific plate and Caroline Plateau, determined the thermal-pressure condition and seismogenic mechanism of earthquakes, and concluded the influences from subduction of the oceanic plateau in the generation of intermediate-depth earthquakes.

2. Tectonic setting and data

The Mariana subduction zone is located at the boundary between the eastern edge of the Philippine Sea Plate and the subducting Pacific Plate. The subduction began in the Eocene prior to about 52 Ma (Arculus et al., 2015). The subducted plate rolled back while it was pinned at the northern and southern ends of the trench system by the impinging Ogasawara Plateau and the Caroline Ridge, respectively (Hsui and Youngquist, 1985; Moberly, 1972), leading to an eastward bow-shaped geometry of the trench (Fig. 1e, Fig. 2). The northern, central, and southern Mariana Trough thus experienced different modes of opening, resulting in significant variations in seismicity and geological structure along the strike of the subduction zone (Sleeper et al., 2021). The Mariana subduction zone is a water-rich system, as indicated by the presence of serpentinite lithospheric mantle in both central and southern Mariana Trench, as revealed by seismic tomography results (Cai et al., 2018; Pozgay et al., 2009; Pyle et al., 2010; Wan et al., 2019; Zhu et al., 2021).

The southern end of the Mariana Trench is connected with the Yap Trench at around 11.16° N, where the Caroline Plateau subducts beneath the Philippine Sea Plate at an extremely slow convergence velocity of <1 cm per year (Kotake, 2000; Seno et al., 1993). The Caroline Plateau was formed by mantle plume activity between 33 and 15 million years ago (Zhang et al., 2023a). The initiation of the collision is yet well-determined, ranging from the late Oligocene to the middle Miocene (Dong et al., 2018; Fujiwara et al., 2000). It is a topography high located on the Caroline Plate, which was formed by hotspot activity in the late Oligocene (Keating et al., 1984; Weissel and Anderson, 1978). As such, the Caroline Plateau is characterized as a young, buoyant oceanic plateau with an over-thickened crust (Gan et al., 2021), contrasting with the older and relatively thinner Pacific oceanic crust to its north. Lee (2004) suggested that the subduction of the thick Caroline Plateau and the slow convergence velocity might result in a lack of intermediate-depth earthquakes in the region.

We utilized seismic data collected from a passive-source OBS experiment, which contains 5 three-component OBSs, conducted from 5

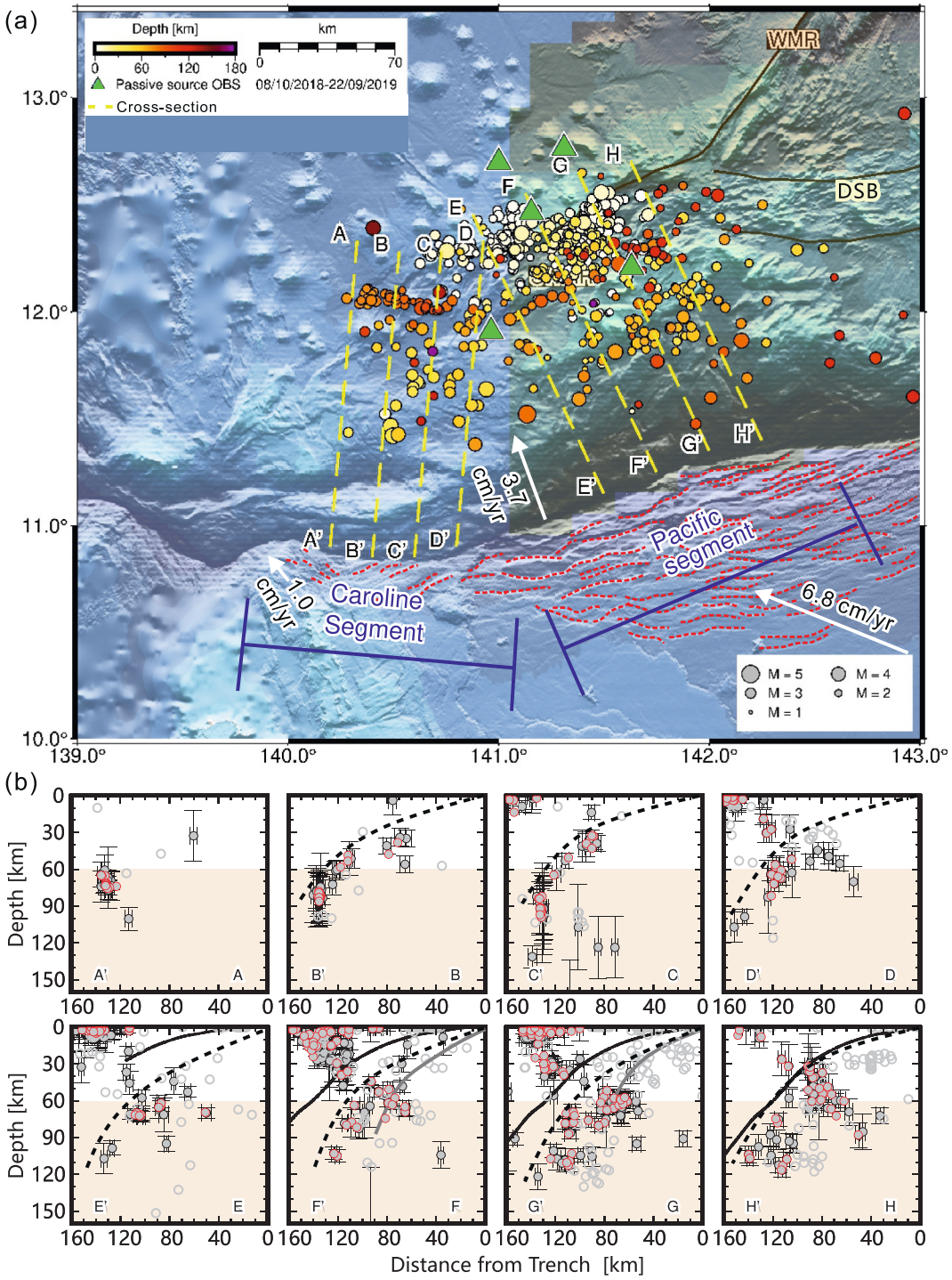

Fig. 3. (a) Map of absolute earthquake locations (circles) colored by depth based on the OBS (green triangles) observation in the southernmost Mariana subduction zone. The shaded area shows the subducted slab from slab 2.0 model (Hayes, 2018). The red dashed lines represent the major faults in the outer-rise regions. The dashed yellow lines represent the cross-sections. The white arrows indicate the subduction rate of the slab (Kotake, 2000; Lee, 2004; Schellart, 2023). (b) Cross-section views with a bin width of 20 km of earthquakes (gray open circles) with locations shown in panel (a) as well as earthquakes relocated using the double-difference (hypoDD) method (red circles). The location errors in vertical and horizontal directions were plotted as error bars. Trench locations are marked as 0 km. The gray circles represent earthquakes in (Chen et al., 2022) catalog. The pink area denotes the intermediate depth range. The black dashed line shows the boundary of the subducted slab as depicted by earthquake locations and black line shows that from slab 2.0 model. The dark gray lines in cross-section F,G represent the plate boundaries from (Wang et al., 2024). The geometry of the subducting slab is better constrained by our localization data. WMR, West Mariana Ridge; DSB, Diffuse spreading belt. (For interpretation of the references to colour in this figure legend, the reader is referred to the web version of this article.)

September 2018 to 22 October 2019 (Fig. 2). These data were collected by the R/V *Tan Suo Yi Hao* and *Shi Yan San Hao*. Unlike previous OBS experiments in the southern Mariana region (Chen et al., 2022), the array in this study was situated on the overriding plate near the Southwest Mariana Rift (SWMR) and operated continuously for over a year. Time-drifting issues of the instruments were corrected by employing the ambient noise cross-correlation method (Abbas et al., 2023).

3. Methods and results

3.1. Earthquake detection, location, and magnitude calibration

We applied the EQTransformer method (Mousavi et al., 2020) to three-component continuous waveforms filtered at 1 Hz high-pass, using default probability thresholds (0.1 for event detection and 0.3 for phase picking), as validated by previous tests (Chen et al., 2022). We used the hydrophone component of the OBS H34 instead of its low signal-to-noise ratio vertical component. The detected phases were then associated using the REAL method (Zhang et al., 2019) within a searching volume of 1 degree in horizontal directions and 200 km in depth around the OBS station, which recorded the first P-arrival, with grid sizes of 0.05 degrees and 10 km in horizontal and vertical directions, respectively. The thresholds of P-, S-, and total arrivals were set as 2, 2, and 5, respectively. We used the IASP91 global velocity model (Kennett and Engdahl, 1991) in phase association. Given the expected deviations from the IASP91 global velocity model (Kennett and Engdahl, 1991) in the study region, we adopted relatively large time windows (1.5 s for P-waves and 2.5 s for S-waves) during phase association. 16,577 P- and 17,531 S-wave phases were detected (Fig. S1), among which 3942 P- and 3819 S-wave phases were associated, generating 1172 events.

To eliminate earthquake location errors caused by picking errors and to exclude false events, we manually corrected the phases picked by EQTransformer after denoising the waveforms using a continuous wavelet-transform-based seismic method (Mousavi, 2016). For both P- and S-wave arrivals, about 1/3 of P- and S-wave arrivals were corrected, with 16.8 % and 13.6 % showing errors over 1 s (Fig. S3). Such picking errors could introduce several kilometers of location errors. Subsequently, the earthquakes were located using both absolute and relative earthquake location methods. During the earthquake location process, we first constructed a localized 1D velocity model for the study region (Fig. S4) by combining the upper 70 km from a 1D velocity structure (Wan et al., 2019) with the deeper part of the IASP91 global velocity model (Kennett and Engdahl, 1991). Then, using the Hypoinverse program (Klein, 2002), we located the detected events based on the P- and S-wave arrivals. We finally obtained a local earthquake catalog containing 613 well-located earthquakes (with location errors of less than 10 km and RMS values of less than 1 s) (Fig. 3a), including shallow intraplate events, interplate events, and intermediate-depth earthquakes. Using the HypoDD method (Waldhauser and Ellsworth, 2000), 385 of these events were further refined based on differential times (Fig. S5, red dots). Detailed descriptions of HypoDD relocation are provided in Text S1. Compared to the results from Chen et al. (2022) (gray open circles in Fig. 3b), our observations in the Caroline segment detected a significantly greater number of earthquakes (gray solid circles), providing enhanced constraints for analyzing seismic distribution characteristics.

After that, we calculated the magnitudes of the events based on the amplitude ratio as follows:

$$M = M_{template} + C\log_{10}R \quad (1)$$

where $M_{template}$ is the magnitude of the closest USGS events, C is a constant, and R is the amplitude ratio between the target event and the template (Schaff and Richards, 2014). We took C = 1 because we adopted the template event's local magnitude (Shelly et al., 2016). Events from the USGS catalog during the instrument deployment time were used as templates. The magnitude of detected events ranges from 1.5 to 5.2. No significant differences were observed between the two segments, with a minimum magnitude of 1.7 in the Caroline segment and 1.5 in the Pacific segment.

Bootstrapping (Billings et al., 1994) and jackknifing techniques (Tichelaar and Ruff, 1989) were used to estimate uncertainties of Hypoinverse and HypoDD results, respectively. Hypoinverse location uncertainties for the majority of events were constrained to <5 km horizontally (both *E*-W and N-S components) and < 10 km vertically (Figs. S5, S6 a, b, c). For the HypoDD results, most events exhibited location uncertainties of <2 km horizontally and < 3 km vertically (Refer to Text S2.1 and Fig. S6). To evaluate the effects of limited azimuthal station coverage inherent to our network geometry, we conducted synthetic earthquake tests. The results show that the inclined distribution of earthquakes can be constrained effectively with the current network coverage (Refer to Text S2.2 and Fig. S7). In addition, we assessed whether the different numbers of earthquakes in two segments come from differences in station number (i.e., detection capability) (Refer to Text S2.3 and Fig. S8).

3.2. The along-strike variation of Intermediate-depth earthquake

Significant along-strike variation of intermediate-depth earthquakes was observed in earthquake location results. Here, we defined two segments of the subduction zone as the Caroline and Pacific segments corresponding to the Caroline Plateau and Pacific Plate (Fig. 3a). We projected the relocated hypocenters onto eight 20-km-wide cross-sectional profiles (yellow dashed lines in Fig. 3a) to analyze the earthquake distribution characteristics. The cross-section views show that IDE activities varied in the two subduction segments in terms of the number of events as well as the thickness of the seismicity zones. In profiles A-D, earthquake depths systematically decrease westward. We demonstrate that this pattern cannot be explained by seismic network coverage limitations, as evidenced by our detection of earthquakes >120 km depth east of profile H at comparable network distances. This observed along-strike shallowing of seismicity reflects corresponding variations in slab geometry, indicating significantly shallower subduction in the western segment. This observation aligns with the expected behavior of younger slabs, which exhibit higher thermal buoyancy (Kirby et al., 1996a; Bina et al., 2001; Gan et al., 2021).

In general, the subducted slab in the Caroline segment experienced fewer Intermediate-depth earthquake activities that extend to around 120 km depth, showing a concentrated single seismicity zone with a thickness of around 20 km, compatible with the 20 km average crustal thickness in the Caroline Ridge region (Altis, 1999). To the Pacific segment, the IDE seismicity increased significantly, showing a scattered seismicity zone with a thickness of around 50 km that extends to around 130 km depth. According to previous observations (Abers, 1992; Hasegawa et al., 1978; Kawakatsu, 1986; Shiobara et al., 2010), at regions where DSZs existed, the thickness of seismogenic zones (from upper layer to lower layer) was typically larger than 30–40 km. The approximately 50 km thick seismogenic zone observed in the Pacific segment substantially exceeds the thickness of typical oceanic crust (~8 km; Wan et al., 2019), demonstrating that seismic activity extends through both the subducted crust and upper mantle lithosphere.

Our relocation results did not reveal two distinct, well-separated seismic layers—likely due to limitations in recording duration and location accuracy. We thus evaluated the potential existence of DSZs using the methodology established by Brudzinski et al. (2007), which has been successfully applied in multiple local seismic network studies (Sippl et al., 2019; Wei et al., 2017). The method rotates the slab in the horizontal direction to obtain the slab-normal distribution of intermediate-depth earthquakes. Then, it checks the existence of DSZs by using dip testing, which determines whether there is a multimodal distribution in the histogram (Hartigan and Hartigan, 1985). We first

determined the rotation angle in the Caroline segment and the Pacific segment (65° and 50°) based on the slab geometry depicted in the cross-section views (Fig. 4a, b). Due to the absence of the slab 2.0 model data (Hayes, 2018) in the Caroline segment (Fig. 3b) and large location errors in the global earthquake catalog for this area, we were previously unable to identify the geometry of the subduction plate. In comparison, the subducted plate can be clearly delineated based on our improved earthquake distribution (Fig. 3b, Fig. 4a).

We then calculated the slab-normal distribution of intermediate-depth earthquakes across all cross-sections and aggregated them for each region. Beneath the Pacific segment, there are two obvious peaks of the number of earthquakes (Fig. 4d), separated by approximately 20 km. In contrast, only a single peak is observed beneath the Caroline segment (Fig. 4c). We performed the same process using earthquakes from the long-term USGS catalog, but the pattern did not show a single-peak or double-peak feature (Fig. S9), which is likely caused by large location errors (up to 100 km) of the global catalog (Fig. S10) in the study region as demonstrated in Text S3. To further analyze the depth pattern of our observed seismicity, we applied Gaussian Mixture Modeling (GMM) (Reynolds, 2009; Seydoux et al., 2020) to assess whether the seismicity distributions in two regions form distinct layers. The GMM results reveal distinct stratification patterns between segments. In the Pacific segment, Intermediate-depth earthquakes separate into two statistically distinct clusters with inter-layer spacing around 20 km, while in the Caroline segment, seismicity forms a single cluster (Fig. S11, S12). This finding provides independent evidence supporting the existence of DSZs in the Pacific segment.

4. Discussion

4.1. Correlation between seismic patterns and the plate tectonic features

The variation in intermediate-depth earthquake patterns beneath the Pacific and Caroline segments is likely related to different structural features of the incoming plate, including bending faults and plate topography. The Caroline Plateau is located in the outer rise of the Caroline segment and experienced plateau-arc collision (Zhang et al., 2023a, 2023b) (Fig. 2). Bathymetric data show fewer outer-rise faults in the Caroline segment compared to the Pacific segment (Fig. 2, S10a). In contrast, the Pacific oceanic plate subducts in the Pacific segment, creating extensive outer-rise faults (Fig. 2) (Chen et al., 2022; Zhu et al., 2021). We identified potential normal faults in cross-section and map views of high-resolution bathymetric data (Fig. S13). In total, there were 41 faults identified from the high-resolution bathymetric data in the Caroline segment, while 129 faults were identified in the Pacific segment. The number of intermediate-depth earthquakes in both segments (261 in the Caroline and 525 in the Pacific segment) is closely proportional to the number of faults (Fig. S10c, blue line and red line). In addition, the peaks in the slab-normal distribution of intermediate-depth earthquakes in two segments (15 km and 30 km) match well with the fault development depth (Fig. 4c, d). For plateau subduction (Caroline segment), Zhang et al. (2022) note that the subduction of an oceanic plateau results in fewer and shallower normal outer-rise faults (around 10–15 km). The deepest outer-rise fault in the Pacific segment reaches the lithospheric mantle (~30 km), supported by numerical

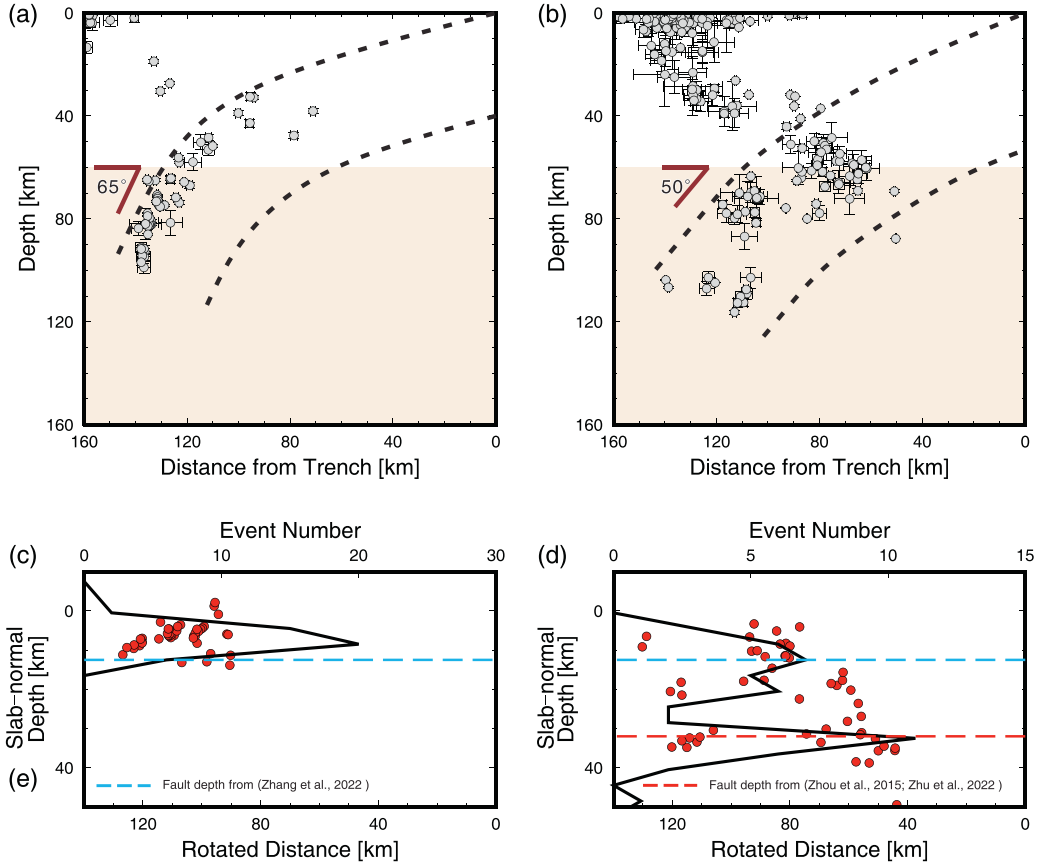

Fig. 4. (a) The combined projection of intermediate-depth earthquakes in the Caroline segment. The black dashed line shows the boundary of the subducted slab as depicted by earthquake locations. Earthquake location uncertainties (error bars) derived from the bootstrapping of HypoDD location. (b) The same as figure (a), but for the Pacific segment (c) The rotated combined projection of intermediate-depth earthquakes from HypoDD result (red circles) in the Caroline segment, the black line represents the number of rotated events with a bin width of 4 km. (d) The same as figure (c), but for the Pacific segment. The blue dashed line shows the fault depth simulated by Zhang et al. (2022), while the red dashed line represents the fault depth revealed by numerical simulations and surface wave imaging (Zhou et al., 2015; Zhu et al., 2021). (For interpretation of the references to colour in this figure legend, the reader is referred to the web version of this article.)

modeling, ambient noise tomography, and earthquake studies (Chen et al., 2022; Zhou et al., 2015; Zhu et al., 2021).

Previous studies showed that well-developed bending faults lead to more extensive plate hydration (Boneh et al., 2019; Geersen et al., 2022) as outer-rise faults serve as pathways for water to infiltrate into the subducting plate (Ranero et al., 2003). We thus estimated serpentinization of the subducted slab by calculating the water-penetrated fault zone volume along each cross-section (Text S4). The serpentinized volume was calculated by multiplying the parameters by fault counts. The estimation shows that the average serpentinized volume was around 76–615 km^3 and 725–5805 km^3 in the Caroline and Pacific segments, respectively (Fig. S14c). The Pacific segment carries about ten times more water than the Caroline segment. Besides, both active-source seismic tomography (Contreras-Reyes, 2025; He et al., 2023; He et al., 2025; Li et al., 2023; Wan et al., 2019) and ambient noise tomography (Zhu et al., 2021) in our study region revealed low-velocity anomalies in the outer rise and near-trench regions, suggesting a higher degree of slab hydration. Although a tomography study is lacking in the Caroline segment, the multi-channel seismic profiles reveal that the faults in this area are relatively shallowly developed, suggesting lower slab hydration levels (Zhang et al., 2021). These results provide additional evidence for distinct hydration states between the two segments.

In summary, the number of intermediate-depth earthquakes increases from the Caroline to the Pacific segments, corresponding to the increase in outer-rise faults and estimated slab hydration volume. The peaks in the slab-normal distribution of intermediate-depth earthquakes closely match the depths of outer-rise faults identified in previous research (Zhang et al., 2022; Zhou et al., 2015; Zhu et al., 2021).

4.2. The thermal and pressure conditions of intermediate-depth earthquakes

The thermal and pressure condition of the subducted slab significantly influences the occurrence of mineral phase change and dehydration processes (Abers et al., 2006), thus playing an important role in intermediate-depth earthquake generation (Hacker et al., 2003; Peacock, 2003; van Keken et al., 2012). To verify the thermal control of intermediate-depth earthquake genesis and to distinguish the patterns of subducted plate affiliations, we analyzed the thermal-pressure structure of both segments. The temperature distribution in the two segments was obtained by solving the thermal-kinetic equation, considering a given velocity field (Negredo et al., 2004; Peacock, 2003, 2020; van Keken et al., 2008), with the velocity field described by the analytical expression provided by Negredo et al. (2004). The slab age, slab dip, convergence rate, and shear heating are the most important factors controlling the slab's thermal structure (Peacock, 2003, 2020; van Keken et al., 2008). Shear heating was not included in the thermal model calculation because it only has a minor effect on the thermal structure and is limited to regions close to the shear zone (Yamasaki and Seno, 2003).

Due to the pronounced correlation between seismic distribution patterns and plate structural characteristics, we inferred that the subducted plate in the Caroline segment corresponds to the Caroline Plateau, not the Pacific plate. In our model, the ages of the Pacific and Caroline segments are set to 125 Ma (Xu et al., 2023) and 20 Ma (Zhang et al., 2023a) respectively, with vertical subduction rates of 3.7 cm/yr (Schellart, 2023) and 1.0 cm/yr (Kotake, 2000; Lee, 2004) respectively. For the dip angles in the intermediate-depth range, we determined them based on the earthquake location results. The dip angle is set as 50° and 65° for the Pacific and Caroline segments according to our location results, respectively. The initial temperature structure is calculated using the thermal plate model GDH1 by Stein and Stein (1994). In addition, we also consider the scenario where the subducting plates in the Caroline segment are part of the Pacific Plate, differing from the Pacific segment only in dip angle (Fig. S15a). The potential existence of a Caroline mantle plume (Zhong et al., 2025) may thermally perturb the local mantle. Following (Zhang et al., 2023b), we therefore conducted additional numerical tests (Fig. S15c) with an elevated mantle temperature of 1550 °C (compared to the baseline 1450 °C model).

To assess the uncertainties introduced by parameter selection, we performed comprehensive thermal modeling of the subducting slabs by varying three key parameters: slab age, convergence rate, and dip angle. For the Pacific segment, we tested slab ages of 105, 115, 125, and 135 Ma; convergence rates from 3.0 to 4.0 cm/yr in 0.2 cm/yr increments; and dip angles of 45°, 50°, and 55°, resulting in 72 parameter combinations. For the Caroline segment, we considered slab ages (15, 20, and 25 Ma), convergence rates (0.8, 1.0, and 1.2 cm/yr), and dips (60°, 65°, and 70°), generating 27 distinct models. Due to the Yap slab's younger age and slower subduction velocity, the limited parameter variations in our tests already cover a significant portion of its plausible thermal-pressure range. We analyzed the temperature-pressure (P-T) conditions of earthquakes across all model configurations, assigning each event an uncertainty range of ±2 standard deviations (error bars in Fig. 5c, d). The results reveal maximum temperature uncertainties reaching ~200 °C, predominantly observed for high-pressure (i.e., deeper) earthquakes. This significant thermal variability is primarily generated from dip angle variations because variations in slab dip angle induce larger displacements in slab position at greater depths. In contrast, uncertainties induced by slab age and convergence rate variations remain comparatively minor, particularly for shallow earthquakes (lower pressure regimes).

The locations of intermediate-depth earthquakes in both the Caroline and Pacific segments were mapped onto the thermal contours (Fig. 5a, b). Generally, most of the intermediate-depth earthquakes are located within the region under a temperature of 600 degrees Celsius and the maximum depth of the intermediate-depth earthquakes increases with the subduction thermal parameter, which is calculated based on slab age, convergence velocity, and slab dip angle (Kirby et al., 1996b). In the Caroline segment, the P-T range for intermediate-depth earthquakes is approximately 400–600 °C and 1.5–3.4 GPa. In the Pacific segment, the upper plane seismicity exists under P-T conditions of about 200–400 °C and 1–3.6 GPa, while the lower plane seismicity is found within a P-T range of 400–600 °C and 2–3.8 GPa. The temperature range for the lower plane seismicity matches the findings reported by Aziz Zanjani et al. (2021).

We superimposed the intermediate-depth earthquakes of the Caroline segment and the upper layers of the Pacific segment onto the phase diagram from Hacker et al. (2003) (Fig. 5c). These events are chiefly located in the hydration path of the hydrous minerals, suggesting that the dehydration of blueschists in the oceanic crust might be the seismogenesis of these events. In the Caroline segment, Lawsonite blueschists transform into amphibole-eclogite facies and then into zoisite eclogite facies as P-T increases from approximately 300 °C and 1.5–2 GPa to 600 °C and around 3 GPa. In the Pacific segment, Lawsonite blueschists transform into jadeite-lawsonite blueschist facies and subsequently into Lawsonite amphibole-eclogite facies as P-T increase from approximately 175 °C and 1–1.5 GPa to 400 °C and around 3.5 GPa. The distribution of the intermediate-depth earthquakes in the Caroline and Pacific segments also aligns with the P-T regimes of intermediate-depth earthquakes in the Tohoku upper zone and Costa Rica. The correlation is not perfect, suggesting potential uncertainties in the locations of the earthquakes, thermal modeling, or petrological modeling. In the scenario where the subducting plates in the Caroline segment are part of the Pacific Plate (Fig. S15a, b), the intermediate-depth earthquakes are located in two-phase change paths mentioned above, which seems inconsistent with the spatial distribution of intermediate-depth earthquakes concentrated in the Caroline segment. Furthermore, if the presence of a mantle plume elevates mantle temperatures, our modeling results demonstrate that this has minimal impact on the thermopressure conditions governing intraslab seismicity (Fig. S15c, d).

The lower plane seismicity in the Pacific segment occurs in the plate mantle, where the principal hydrous minerals are serpentine (antigorite) and chlorite. We superimposed these intermediate-depth earthquakes

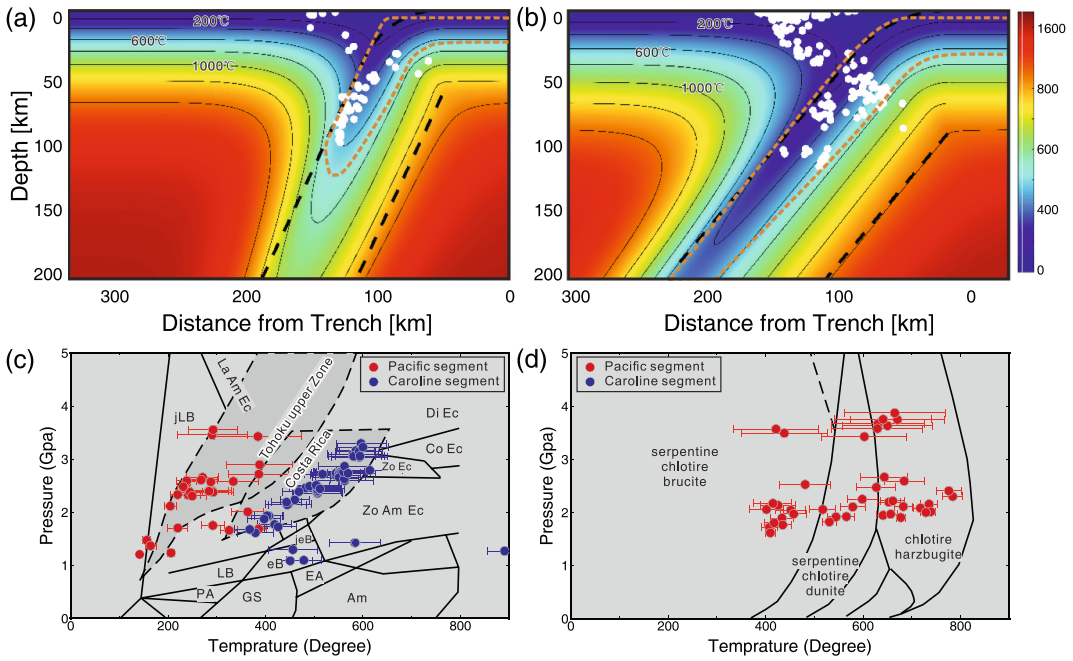

Fig. 5. (a) The 4 cross-sections combined projection of intermediate-depth earthquakes from HypoDD results in the Caroline segment. The contours denote the slab temperature with an interval of 200 °C, the dashed orange lines mark the antigorite stability (Schmidt and Poli, 1998), and the dashed black lines depict the subducted slab. (b) The same as figure (a), but for the Pacific segment. (c) Pressure-temperature (P-T) conditions of intermediate-depth earthquakes of the Caroline segment and upper plane of the Pacific segment. The background phase diagram is from (Hacker et al., 2003), and the dots indicate the P-T conditions of intermediate-depth earthquakes. Temperature uncertainties are displayed by error bars. (d) The same as figure (c), but for the lower plane intermediate-depth earthquakes of the Pacific segment. Abbreviations: PA: prehnite-actinolite facies; GS: greenschist facies; EA: epidote-amphibolite facies; AM: amphibolite facies; EA: epidote amphibolite; BS: blueschist facies; eB: epidote blueschist; jeB: jadeite-epidote blueschist facies; jLB: jadeite-lawsonite blueschist facies; Am Ec: amphibole eclogite facies; Zo: zoisite; and Co: coesite.

onto the metamorphic facies for harzburgite (Hacker et al., 2003) (Fig. 5d). Those events also correlate spatially with the phase change path of serpentine, showing a contribution from the dehydration of serpentine, as suggested by Hacker et al. (2003). Given the strong correlation between lower-plane seismicity and outer-rise plate hydration reaching the mantle, we suggest that lower-plane seismicity is also caused by antigorite dehydration. Notably, Yamasaki and Seno (2003) showed that antigorite is stable under P-T conditions of 400–600 °C and 2–4 GPa. Different reaction boundaries may result from the compositional and structural states of the starting materials (Yamasaki and Seno, 2003). Additionally, observations of the dry lithospheric mantle (and the lower layer of DSZs) in studies (Fang and van der Hilst, 2019; Florez and Prieto, 2019) challenge the dehydration embrittlement mechanism, indicating the complexity of the mechanisms underlying lower-layer seismicity.

4.3. *The impact of oceanic plateau on intermediate-depth earthquakes*

Our observations reveal intermediate-depth seismicity patterns that correlate closely with the distinct characteristics of the subducting slab. Besides, the distribution of intermediate-depth earthquakes in the International Seismological Centre catalog shows a sudden change between the Caroline and Pacific segments (Fig. 2) (Lee, 2004). The two main tectonic units in the study area—the Challenger Deep and the Southwest Mariana Rift—are developed only in the Pacific segment, also indicating different tectonic settings in the two segments (Fig. 2). The distinct seismic characteristics, combined with the contrasting features of the subduction zone and back-arc region, as well as the markedly segmented outer-rise morphology between the Pacific and Caroline segments, suggest that differences in subducting plate features are responsible for these pronounced variations. As we inferred, the subducted plate in the Caroline segment corresponds to the Caroline Plateau, not the Pacific plate. This could explain the shallower trench in the Caroline segment, as the greater the age of subducting plate, the greater the trench depth (Fryer et al., 2003; Hilde and Uyeda, 1983). This also explains the lack of a back-arc rift in the Caroline segment, as dehydration-released fluid migration promotes the back-arc spreading (Hanyu et al., 2006; Zhao et al., 1997), but the subducting Caroline plate experiences a lower degree of hydration, dehydration and released fluid migration.

However, since profiles A-D also appear to lie along the current subduction direction of the Pacific slab, how can they be attributed to the subducting Caroline plate? In curved subduction zones, the convex-outward bending of the central subducted slab drives inward motion of both flanking segments, as observed in other subduction zones such as those in Mariana, Alaska, and Sumatra trench from the Slab 2.0 model (Hayes, 2018). What's more, the slab retreating induces toroidal mantle flow (Liu et al., 2019; Zhu et al., 2020), drawing the adjacent slab edges inward. Because the subducted Caroline slab has broken off, revealed by P-wave tomography and Receiver Function analysis results (Fan et al., 2022). Consequently, in our study area, the Caroline Plateau (specifically the North Caroline Ridge) remains structurally connected to the Pacific Plate but has become detached from the Caroline Plate proper. We thus suggest that the combined effects of the strongly curved Mariana Trench geometry and retreating Pacific slab (Hsui and Youngquist, 1985; Moberly, 1972) collectively dragged the Caroline segment into its current position beneath profiles A-D. An alternative explanation is that both segments of the subducting plates belong to the Pacific Plate but have undergone different developments of outer-rise faults and hydration processes. In this scenario, the existence of the Caroline Plateau limits hydration in the outer rise region of the Caroline segment, as the less developed faults are shown in high-resolution bathymetric data.

Based on the above observations and analyses, we propose a conceptual model (Fig. 6) that establishes how hydration heterogeneity coming from different plate structures affects the occurrence and distribution of intermediate-depth earthquakes. The subduction of thin

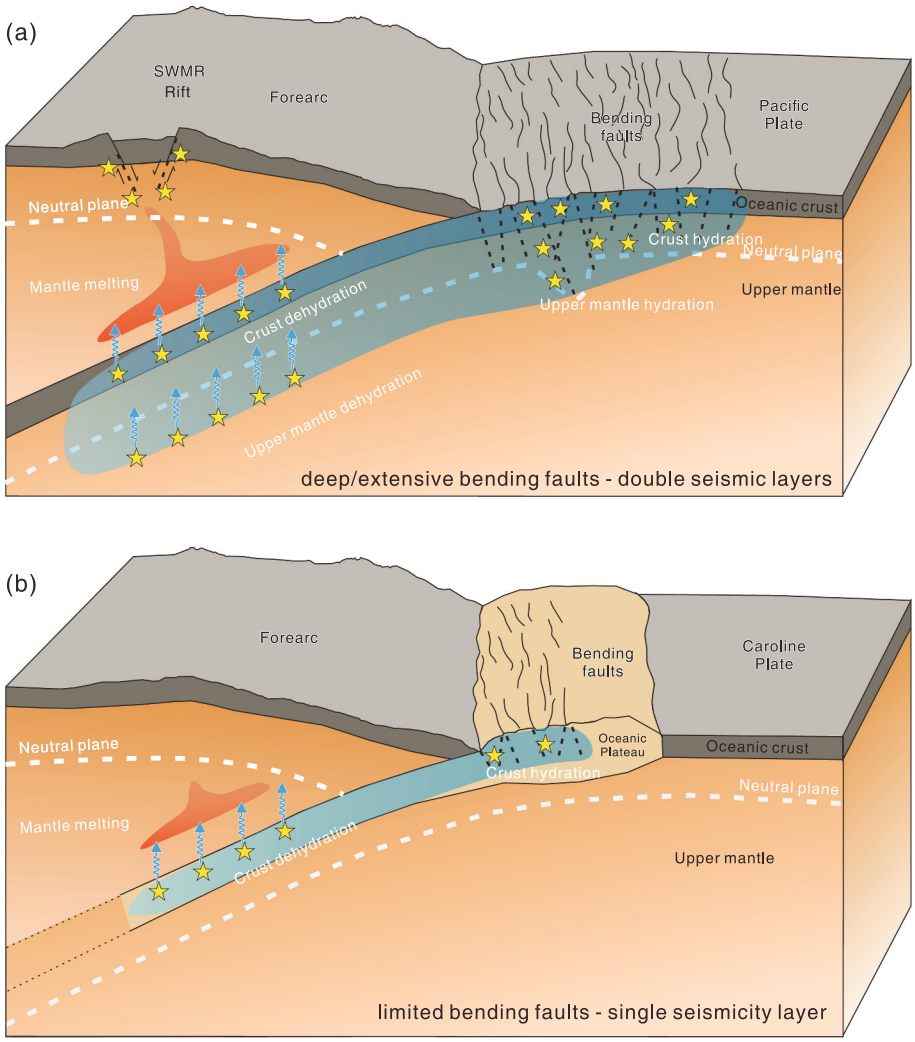

Fig. 6. Cartoon figures illustrate the relationship among the slab topography, the outer-rise faulting, plate hydration-dehydration, and the occurrence of intermediate-depth earthquakes for oceanic plate subduction (a) and plateau subduction (b) segments. Black dashed lines represent the faults. The yellow dashed line represents the lower boundary of the oceanic crust, and the white dashed lines represent the boundary of the lithospheric mantle. Blue-shadowed regions indicate the hydrated material and blue arrows denote the fluid release. The yellow stars correspond to earthquakes. The brown areas represent the melting mantle material. (For interpretation of the references to colour in this figure legend, the reader is referred to the web version of this article.)

oceanic slabs with well-developed outer-rise faults leads to a higher degree of slab hydration. This hydrated slab subsequently dehydrated, triggering more active intermediate-depth earthquakes and the formation of DSZs (Fig. 6a). In contrast, the subduction of thick oceanic plateaus produces limited outer-rise faulting, restricting plate hydration to shallow levels. The absence of deep dehydration reactions prevents lower-layer seismicity and formation of SSZ (Fig. 6b). Our results suggest that outer-rise hydration significantly influences the generation and distribution of intermediate-depth earthquakes, which agrees with previous studies (Nakajima, 2019; Shillington et al., 2015; Wei et al., 2021).

It should be noted that the limited one-year duration and restricted spatial coverage of our dataset may not comprehensively represent the full spectrum of seismic distributions. To achieve more comprehensive results, future studies should employ expanded seismic networks with broader spatial coverage and longer monitoring periods. Investigating subduction zones with diverse shallow structures – including the northern Mariana (oceanic plateau), Sumatran and western Alaskan, and Peruvian (mid-ocean ridge) subduction zones - will provide a more comprehensive framework for understanding intermediate-to-deep focus earthquake generation mechanisms. Additionally, further investigation into the focal mechanisms of intermediate-depth earthquakes in situ is essential to advance our understanding of the physical conditions and seismogenic mechanisms within subduction zones.

5. Conclusions

A one-year OBS experiment was conducted at the southernmost Mariana subduction zone with an array of 5 OBSs during the period from 5 September 2018 to 22 October 2019. Using the OBS data, we performed a machine-learning-based earthquake detection method (EQTransformer) and the seismic phase association (REAL) method. We finally located 613 earthquakes utilizing the Hypoinverse and HypoDD algorithms. The observation identifies the variations in the distribution patterns of intermediate-depth earthquakes at the junction of the Pacific plate and the Caroline Plateau. Double seismic zones were observed in the Pacific segment, while a single seismic zone was found in the Caroline segment. The result reveals spatially varied single and double seismicity layers of intermediate-depth earthquakes in the southernmost Mariana Trench, which is consistent with the along-strike variations in subducted slab features. Besides, the thermal-pressure modeling results of the slab suggest that dehydration of hydrous minerals (blueschists, antigorite, etc.) drives intermediate-depth earthquake generation in the study area. Combined with the regional tectonic setting, the results

suggest that the subducting oceanic plateaus generate distinct patterns of bending-related outer-rise faulting versus normal oceanic crust, which in turn causes plate hydration heterogeneity and influences the distribution of intermediate-depth earthquakes.

CRediT authorship contribution statement

Han Chen: Writing – review & editing, Writing – original draft, Visualization, Methodology, Investigation, Formal analysis. **Gaohua Zhu:** Writing – review & editing, Visualization, Supervision, Methodology, Funding acquisition, Formal analysis, Conceptualization. **Hongfeng Yang:** Writing – review & editing, Validation, Supervision, Funding acquisition, Conceptualization. **Jiangyang Zhang:** Writing – review & editing, Writing – original draft, Visualization, Methodology, Formal analysis. **Shaopin Lu:** Writing – review & editing, Data curation. **Chuanxu Chen:** Validation, Data curation. **Jian Lin:** Validation, Data curation. **Yiming Luo:** Writing – review & editing, Visualization.

Declaration of competing interest

The authors declare that they have no known competing financial interests or personal relationships that could have appeared to influence the work reported in this paper.

Acknowledgments

The authors are grateful to the science parties and crew members of R/V *Tan Suo Yi Hao* and *Shi Yan San Hao* for deploying and collecting the OBS instruments. This work was supported by the National Key Research and Development Program of China (Grant No. 2023YFF0806400), the National Natural Science Foundation of China (Nos. 92158205, 91858207, 9215820007, 41890813, 42074123, 42230805, 42406064), the China Postdoctoral Science Foundation (Nos. 2023M741525), Hong Kong Research Grant Council Grants (No. 14304820), Faculty of Science at CUHK, Shenzhen Science and Technology Innovation Commission (Nos. JCYJ20220818100417038, KCXFZ20211020174803005), and Chinese Academy of Sciences (Y4SL021001).

Appendix A. Supplementary data

Supplementary data to this article can be found online at https://doi.org/10.1016/j.tecto.2025.230875.

Data availability

The waveform data used for earthquake detection, location, and magnitude calibration in the study are available at figshare via Chen (2023) with license CC BY 4.0.

References

Abbas, A., Zhu, G., Zi, J., Chen, H., Yang, H., 2023. Evaluating and correcting short-term clock drift in data from temporary seismic deployments. Earthq. Res. Adv. 3 (2), 100199.
Abers, G.A., 1992. Relationship between shallow-and intermediate-depth seismicity in the eastern Aleutian subduction zone. Geophys. Res. Lett. 19 (20), 2019–2022.
Abers, G.A., van Keken, P.E., Kneller, E.A., Ferris, A., Stachnik, J.C., 2006. The thermal structure of subduction zones constrained by seismic imaging: implications for slab dehydration and wedge flow. Earth Planet. Sci. Lett. 241 (3–4), 387–397.
Aki, K., Lee, W., 1976. Determination of three-dimensional velocity anomalies under a seismic array using first P arrival times from local earthquakes: 1. A homogeneous initial model. J. Geophys. Res. 81 (23), 4381–4399.
Altis, S., 1999. Origin and tectonic evolution of the Caroline Ridge and the Sorol Trough, western tropical Pacific, from admittance and a tectonic modeling analysis. Tectonophysics 313 (3), 271–292.
Arculus, R.J., Ishizuka, O., Bogus, K.A., Gurnis, M., Hickey-Vargas, R., Aljahdali, M.H., Bandini-Maeder, A.N., Barth, A.P., Brandl, P.A., Drab, L., do Monte Guerra, R., Hamada, M., Jiang, F., Kanayama, K., Kender, S., Kusano, Y., Li, H., Loudin, L.C., Maffione, M., Marsaglia, K.M., McCarthy, A., Meffre, S., Morris, A., Neuhaus, M., Savov, I.P., Sena, C., Tepley Iii, F.J., van der Land, C., Yogodzinski, G.M., Zhang, Z., 2015. A record of spontaneous subduction initiation in the Izu–Bonin–Mariana arc. Nat. Geosci. 8 (9), 728–733.
Aziz Zanjani, F., Lin, G., Thurber, C.H., 2021. Nested regional-global seismic tomography and precise earthquake relocation along the Hikurangi subduction zone, New Zealand. Geophysical Journal International 227 (3), 1567–1590.
Billings, S., Sambridge, M., Kennett, B., 1994. Errors in hypocenter location: picking, model, and magnitude dependence. Bull. Seismol. Soc. Am. 84 (6), 1978–1990.
Bina, C.R., Stein, S., Marton, F.C., Van Ark, E.M., 2001. Implications of slab mineralogy for subduction dynamics. Phys. Earth Planet. Inter. 127, 51–66.
Boneh, Y., Schottenfels, E., Kwong, K., van Zelst, I., Tong, X., Eimer, M., Miller, M.S., Moresi, L., Warren, J.M., Wiens, D.A., Billen, M., Naliboff, J., Zhan, Z., 2019. Intermediate-depth earthquakes controlled by incoming plate hydration along bending-related faults. Geophys. Res. Lett. 46 (7), 3688–3697.
Brudzinski, M.R., Thurber, C.H., Hacker, B.R., Engdahl, E.R., 2007. Global prevalence of double Benioff zones. Science 316 (5830), 1472–1474.
Cai, C., Wiens, D.A., Shen, W., Eimer, M., 2018. Water input into the Mariana subduction zone estimated from ocean-bottom seismic data. Nature 563 (7731), 389–392.
Chen, 2023. SWMR-IDEs-events-data. Figshare. [Dataset]. https://doi.org/10.6084/m9.figshare.24458869.v1.
Chen, H., Yang, H., Zhu, G., Xu, M., Lin, J., You, Q., 2022. Deep outer-rise faults in the Southern Mariana Subduction Zone indicated by a machine-learning-based high-resolution earthquake catalog. Geophys. Res. Lett. 49 (12) (p. e2022GL097779).
Christova, C., Scholz, C.H., 2003. Stresses in the Vanuatu subducting slab: a test of two hypotheses. Geophys. Res. Lett. 30 (15).
Contreras-Reyes, E., 2025. Commentary: intense upper mantle hydration of the Pacific Plate beneath the southern Mariana Trench. Geophys. Res. Lett. 52 (e2025GL116626).
Dong, D., Zhang, Z., Bai, Y., Fan, J., Zhang, G., 2018. Topographic and sedimentary features in the Yap subduction zone and their implications for the Caroline Ridge subduction. Tectonophysics 722, 410–421.
Dorbath, C., Gerbault, M., Carlier, G., Guiraud, M., 2008. Double seismic zone of the Nazca plate in northern Chile: high-resolution velocity structure, petrological implications, and thermomechanical modeling. Geochem. Geophys. Geosyst. 9 (7).
Emry, E.L., Wiens, D.A., Garcia-Castellanos, D., 2014. Faulting within the Pacific plate at the Mariana Trench: Implications for plate interface coupling and subduction of hydrous minerals. J. Geophys. Res. 119 (4), 3076–3095.
Engdahl, E.R., Scholz, C.H., 1977. A double Benioff Zone beneath the central Aleutians: an unbending of the lithosphere. Geophys. Res. Lett. 4 (10), 473–476.
Fan, J., Zheng, H., Zhao, D., Dong, D., Bai, Y., Li, C., Zhang, Z., 2022. Seismic structure of the Caroline Plateau-Yap Trench collision zone. Geophys. Res. Lett. 49 (6) (p. e2022GL098017).
Fang, H., van der Hilst, R.D., 2019. Earthquake depth phase extraction with P wave autocorrelation provides insight into mechanisms of intermediate-depth earthquakes. Geophys. Res. Lett. 46 (24), 14440–14449.
Ferrand, T.P., Hilairet, N., Incel, S., Deldicque, D., Labrousse, L., Gasc, J., Renner, J., Wang, Y., Green Ii, H.W., Schubnel, A., 2017. Dehydration-driven stress transfer triggers intermediate-depth earthquakes. Nat. Commun. 8 (1), 1–11.
Florez, M., Prieto, G., 2019. Controlling factors of seismicity and geometry in double seismic zones. Geophys. Res. Lett. 46 (8), 4174–4181.
Frohlich, C., 2006. Deep Earthquakes. Cambridge Univeristy Press, New York.
Fryer, P., Becker, N., Appelgate, B., Martinez, F., Edwards, M., Fryer, G., 2003. Why is the challenger deep so deep? Earth Planet. Sci. Lett. 211 (3–4), 259–269.
Fujiwara, T., Tamura, C., Nishizawa, A., Fujioka, K., Kobayashi, K., Iwabuchi, Y., 2000. Morphology and tectonics of the Yap Trench. Mar. Geophys. Res. 21 (1), 69–86.
Gan, Y., Ma, X., Luan, Z., Yan, J., 2021. Morphology and multifractal features of a guyot in specific topographic vicinity in the Caroline Ridge, West Pacific. J. Oceanol. Limnol. 39 (5), 1591–1604.
Geersen, J., Sippl, C., Harmon, N., 2022. Impact of bending-related faulting and oceanic-plate topography on slab hydration and intermediate-depth seismicity. Geosphere 18 (2), 562–584.
Green, H.W., Houston, H., 1995. The mechanics of deep earthquakes. Annu. Rev. Earth Planet. Sci. 23 (1), 169–213.
Gutenberg, B., Richter, C., 1954. Seismicity of the Earth and Related Phenomena. Princeton Univ. y Press, Princeton, NJ, p. 310.
Hacker, B.R., Peacock, S.M., Abers, G.A., Holloway, S.D., 2003. Subduction factory 2. Are intermediate-depth earthquakes in subducting slabs linked to metamorphic dehydration reactions? J. Geophys. Res. 108 (B1).
Hanyu, T., Tatsumi, Y., Nakai, S.I., Chang, Q., Miyazaki, T., Sato, K., Tani, K., Shibata, T., Yoshida, T., 2006. Contribution of slab melting and slab dehydration to magmatism in the NE Japan arc for the last 25 Myr: constraints from geochemistry. Geochem. Geophys. Geosyst. 7 (8).
Hartigan, J.A., Hartigan, P.M., 1985. The Dip Test of Unimodality: the Annals of Statistics, pp. 70–84.
Hasegawa, A., Umino, N., Takagi, A., 1978. Double-planed structure of the deep seismic zone in the northeastern Japan arc. Tectonophysics 47 (1–2), 43–58.
Hayes, G., 2018. A Comprehensive Subduction Zone Geometry Model: US Geological Survey Data Release. https://doi.org/10.5066/F7PV6JNV.
He, E., Qiu, X., Chen, C., et al., 2023. Deep crustal structure across the challenger deep: tectonic deformation and strongly serpentinized layer. Gondw. Res. 118, 135–152.
He, E., Qiu, X., Li, Y., Grevemeyer, I., Xu, M., Zhao, M., Wang, Y., Chen, C., 2025. Strong serpentinization and hydration in the subducting plate of the Southern Mariana Trench: insights from Vp/Vs ratios. Geophys. Res. Lett. 52 (6) (p. e2024GL113792).
Hilde, T.W., Uyeda, S., 1983. Trench depth: variation and significance: geodynamics of the Western Pacific-Indonesian. Region 11, 75–89.
Hirahara, K., 1977. A large-scale three-dimensional seismic structure under the Japan Islands and the Sea of Japan. J. Phys. Earth 25 (4), 393–417.

Hsui, A.T., Youngquist, S., 1985. A dynamic model of the curvature of the Mariana Trench. Nature 318 (6045), 455–457.
Hudnut, K.W., Taber, J.J., 1987. Transition from double to single Wadati-Benioff seismic zone in the Shumagin Islands, Alaska. Geophys. Res. Lett. 14 (2), 143–146.
Incel, S., Hilairet, N., Labrousse, L., John, T., Deldicque, D., Ferrand, T., Wang, Y., Renner, J., Morales, L., Schubnel, A., 2017. Laboratory earthquakes triggered during eclogitization of lawsonite-bearing blueschist. Earth Planet. Sci. Lett. 459, 320–331.
Isacks, B., Oliver, J., Sykes, L.R., 1968. Seismology and the new global tectonics. J. Geophys. Res. 73 (18), 5855–5899.
Kao, H., Liu, L.-G., 1995. A hypothesis for the seismogenesis of a double seismic zone. Geophys. J. Int. 123 (1), 71–84.
Kao, H., Rau, R.-J., 1999. Detailed structures of the subducted Philippine Sea Plate beneath northeast Taiwan: a new type of double seismic zone. J. Geophys. Res. 104 (B1), 1015–1033.
Kawakatsu, H., 1986. Downdip tensional earthquakes beneath the Tonga Arc: a double seismic zone? J. Geophys. Res. 91 (B6), 6432–6440.
Keating, B., Mattey, D., Helsley, C., Naughton, J., Epp, D., Lazarewicz, A., Schwank, D., 1984. Evidence for a hot spot origin of the Caroline Islands. J. Geophys. Res. 89 (B12), 9937–9948.
Kelemen, P.B., Hirth, G., 2007. A periodic shear-heating mechanism for intermediate-depth earthquakes in the mantle. Nature 446 (7137), 787–790.
Kennett, B., Engdahl, E., 1991. Traveltimes for global earthquake location and phase identification. Geophys. J. Int. 105 (2), 429–465.
Kirby, S., 1995. Interslab earthquakes and phase changes in subducting lithosphere. Rev. Geophys. 33 (S1), 287–297.
Kirby, S.H., Stein, S., Okal, E.A., Rubie, D.C., 1996a. Metastable mantle phase transformations and deep earthquakes in subducting oceanic lithosphere. Rev. Geophys. 34 (2), 261–306.
Kirby, S., Engdahl, R.E., Denlinger, R., 1996b. Intermediate-Depth Intraslab Earthquakes and Arc Volcanism as Physical Expressions of Crustal and Uppermost Mantle Metamorphism in Subducting Slabs, in Subduction Top to Bottom. American Geophysical Union, pp. 195–214.
Klein, F.W., 2002. User's Guide to HYPOINVERSE-2000, A Fortran Program To Solve for Earthquake Locations And Magnitudes: US Geological Survey, 2331-1258.
Kotake, Y., 2000. Study on the tectonics of western Pacific region derived from GPS data analysis. Bull. Earthq. Res. Inst. Univ. Tokyo 75, 229–334.
Lee, S.-M., 2004. Deformation from the convergence of oceanic lithosphere into Yap trench and its implications for early-stage subduction. J. Geodyn. 37 (1), 83–102.
Li, Z., Qiu, X., He, E., et al., 2023. Crustal structures of southmost Mariana Trench revealed by wide-angle seismic profile TS01. Chin. J. Geophys. 66 (11), 4691–4704.
Liu, L., Gao, S.S., Liu, K.H., Li, S., Tong, S., Kong, F., 2019. Toroidal mantle flow induced by slab subduction and rollback beneath the Eastern Himalayan syntaxis and adjacent areas. Geophys. Res. Lett. 46 (20), 11080–11090.
Malatesta, C., Gerya, T., Pittaluga, S., Cabiddu, D., 2024. Intermediate-depth seismicity and intraslab stress changes due to outer-rise faulting. Commun. Earth Environ. 5 (1), 253.
Mark, O.K., Illsley-Kemp, F., Townend, J., Barker, S.J., 2024. Evidence from intermediate-depth earthquakes of slab-derived fluids beneath the Taupō volcanic zone. J. Geophys. Res. 129 (5) (p. e2023JB028586).
McGinty, P., Reyners, M., Robinson, R., 2000. Stress directions in the shallow part of the Hikurangi subduction zone, New Zealand, from the inversion of earthquake first motions. Geophys. J. Int. 142 (2), 339–350.
Moberly, R., 1972. Origin of lithosphere behind island arcs, with reference to the western Pacific. In: Studies in Earth and Space Sciences; A Memoir in Honor of Harry Hammond Hess, 132, pp. 35–55.
Mousavi, S.M., 2016. Hybrid seismic denoising using higher-order statistics and improved wavelet block thresholding. Bulletin of the Seismological Society of America 106 (4), 1380–1393.
Mousavi, S.M., Ellsworth, W.L., Zhu, W., Chuang, L.Y., Beroza, G.C., 2020. Earthquake transformer—an attentive deep-learning model for simultaneous earthquake detection and phase picking. Nat. Commun. 11 (1), 1–12.
Nakajima, J., 2019. Revisiting intraslab earthquakes beneath Kyushu, Japan: effect of ridge subduction on seismogenesis. J. Geophys. Res. 124 (8), 8660–8678.
Negredo, A., Valera, J., Carminati, E., 2004. TEMSPOL: a MATLAB thermal model for deep subduction zones including major phase transformations. Comput. Geosci. 30 (3), 249–258.
Ogawa, M., 1987. Shear instability in a viscoelastic material as the cause of deep focus earthquakes. J. Geophys. Res. 92 (B13), 13801–13810.
Owens, T.J., Zandt, G., Taylor, S.R., 1984. Seismic evidence for an ancient rift beneath the Cumberland Plateau, Tennessee: a detailed analysis of broadband teleseismic P waveforms. J. Geophys. Res. 89 (B9), 7783–7795.
Peacock, S.M., 2003. Thermal structure and metamorphic evolution of subducting slabs. In: Geophysical Monograph-American Geophysical Union, 138, pp. 7–22.
Peacock, S.M., 2020. Advances in the thermal and petrologic modeling of subduction zones. Geosphere 16 (4), 936–952.
Pérez-Forero, D., Koulakov, I., Vargas, C.A., Gerya, T., Al Arifi, N., 2023. Lithospheric delamination as the driving mechanism of intermediate-depth seismicity in the Bucaramanga Nest, Colombia. Sci. Rep. 13 (1), 23084.
Pozgay, S.H., Wiens, D.A., Conder, J.A., Shiobara, H., Sugioka, H., 2009. Seismic attenuation tomography of the Mariana subduction system: Implications for thermal structure, volatile distribution, and slow spreading dynamics. Geochem. Geophys. Geosyst. 10 (4).
Prakash, A., Holyoke, C.W., Kelemen, P.B., Kirby, S.H., Kronenberg, A.K., Lamb, W.M., 2023. Carbonates and intermediate-depth seismicity: stable and unstable shear in altered subducting plates and overlying mantle. Proc. Natl. Acad. Sci. 120 (21) (p. e2219076120).
Prieto, G.A., Florez, M., Barrett, S.A., Beroza, G.C., Pedraza, P., Blanco, J.F., Poveda, E., 2013. Seismic evidence for thermal runaway during intermediate-depth earthquake rupture. Geophys. Res. Lett. 40 (23), 6064–6068.
Pyle, M.L., Wiens, D.A., Weeraratne, D.S., Shore, P.J., Shiobara, H., Sugioka, H., 2010. Shear velocity structure of the Mariana mantle wedge from Rayleigh wave phase velocities. J. Geophys. Res. 115 (B11).
Ranero, C.R., Morgan, J.P., McIntosh, K., Reichert, C., 2003. Bending-related faulting and mantle serpentinization at the Middle America trench. Nature 425 (6956), 367–373.
Ratchkovsky, N.A., Pujol, J., Biswas, N.N., 1997. Stress pattern in the double seismic zone beneath Cook Inlet, south-central Alaska. Tectonophysics 281 (3), 163–171.
Revenaugh, J., Jordan, T.H., 1991. Mantle layering from ScS reverberations: 2. The transition zone. J. Geophys. Res. 96 (B12), 19763–19780.
Reynolds, D., Jain, A., 2009. Gaussian mixture models. In: Li, S.Z. (Ed.), Encyclopedia of Biometrics. Springer, Boston, MA, pp. 827–832. https://doi.org/10.1007/978-0-387-73003-5_196.
Sangana, P., Gao, Q., Li, Z., 2022. The impact of the caroline ridge subduction on the geomorphological characteristics of major landforms in the Yap Subduction Zone. J. Mar. Sci. Eng. 10 (10), 1414.
Schaff, D.P., Richards, P.G., 2014. Improvements in magnitude precision, using the statistics of relative amplitudes measured by cross correlation. Geophysical Journal International 197, 335–350.
Schellart, W., 2023. Subduction Zones: A Short Review: Dynamics of Plate Tectonics and Mantle Convection, pp. 321–355.
Schmidt, M.W., Poli, S., 1998. Experimentally based water budgets for dehydrating slabs and consequences for arc magma generation. Earth Planet. Sci. Lett. 163 (1–4), 361–379.
Seno, T., Stein, S., Gripp, A.E., 1993. A model for the motion of the Philippine Sea Plate consistent with NUVEL-1 and geological data. J. Geophys. Res. 98 (B10), 17,941–17,948. https://doi.org/10.1029/93jb00782.
Seydoux, L., Balestriero, R., Poli, P., Hoop, M.D., Campillo, M., Baraniuk, R., 2020. Clustering earthquake signals and background noises in continuous seismic data with unsupervised deep learning. Nat. Commun. 11 (1), 3972.
Shelly, D.R., Ellsworth, W.L., Hill, D.P., 2016. Fluid-faulting evolution in high definition: connecting fault structure and frequency-magnitude variations during the 2014 Long Valley Caldera, California, earthquake swarm. J. Geophys. Res. 121 (3), 1776–1795.
Shillington, D.J., Bécel, A., Nedimović, M.R., Kuehn, H., Webb, S.C., Abers, G.A., Keranen, K.M., Li, J., Delescluse, M., Mattei-Salicrup, G.A., 2015. Link between plate fabric, hydration and subduction zone seismicity in Alaska. Nat. Geosci. 8 (12), 961–964.
Shiobara, H., Sugioka, H., Mochizuki, K., Oki, S., Kanazawa, T., Fukao, Y., Suyehiro, K., 2010. Double seismic zone in the North Mariana region revealed by long-term ocean bottom array observation. Geophys. J. Int. 183 (3), 1455–1469.
Sippl, C., Schurr, B., John, T., Hainzl, S., 2019. Filling the gap in a double seismic zone: intraslab seismicity in Northern Chile. Lithos 346-347, 105155.
Sippl, C., Dielforder, A., John, T., Schmalholz, S.M., 2022. Global constraints on intermediate-depth intraslab stresses from slab geometries and mechanisms of double seismic zone earthquakes. Geochem. Geophys. Geosyst. 23 (9) (p. e2022GC010498).
Sleeper, J.D., Martinez, F., Fryer, P., Stern, R.J., Kelley, K.A., Ohara, Y., 2021. Diffuse spreading, a newly recognized mode of crustal accretion in the southern Mariana Trough backarc basin. Geosphere 17 (5), 1382–1404.
Stein, C.A., Stein, S., 1994. Comparison of plate and asthenospheric flow models for the thermal evolution of oceanic lithosphere. Geophys. Res. Lett. 21 (8), 709–712.
Tichelaar, B.W., Ruff, L.J., 1989. How good are our best models? Jackknifing, bootstrapping, and earthquake depth. Eos Trans. Am. Geophys. Union 70 (20), 593–606.
van Keken, P.E., Currie, C., King, S.D., Behn, M.D., Cagnioncle, A., He, J., Katz, R.F., Lin, S.-C., Parmentier, E.M., Spiegelman, M., Wang, K., 2008. A community benchmark for subduction zone modeling. Phys. Earth Planet. In. 171 (1), 187–197.
van Keken, P.E., Kita, S., Nakajima, J., 2012. Thermal structure and intermediate-depth seismicity in the Tohoku-Hokkaido subduction zones. Solid Earth 3 (2), 355–364.
Waldhauser, F., Ellsworth, W.L., 2000. A double-difference earthquake location algorithm: method and application to the northern Hayward fault, California. Bull. Seismol. Soc. Am. 90 (6), 1353–1368.
Wan, K., Lin, J., Xia, S., Sun, J., Xu, M., Yang, H., Zhou, Z., Zeng, X., Cao, J., Xu, H., 2019. Deep seismic structure across the southernmost Mariana Trench: implications for arc rifting and plate hydration. J. Geophys. Res. 124 (5), 4710–4727.
Wang, K., 2002. Unbending combined with dehydration embrittlement as a cause for double and triple seismic zones. Geophys. Res. Lett. 29 (18) (p. 36–31–36-34).
Wang, X., Xia, S., Yang, H., Chen, H., Zhao, D., 2024. Structure and dynamics of southern Mariana margin: constraints from seismicity, tomography and focal mechanisms. Tectonophysics 878, 230300.
Wei, S.S., Wiens, D.A., van Keken, P.E., Cai, C., 2017. Slab temperature controls on the Tonga double seismic zone and slab mantle dehydration. Sci. Adv. 3 (1), e1601755.
Wei, S.S., Ruprecht, P., Gable, S.L., Huggins, E.G., Ruppert, N., Gao, L., Zhang, H., 2021. Along-strike variations in intermediate-depth seismicity and arc magmatism along the Alaska Peninsula. Earth Planet. Sci. Lett. 563, 116878.
Weissel, J.K., Anderson, R.N., 1978. Is there a Caroline plate? Earth Planet. Sci. Lett. 41 (2), 143–158.
Wiens, D.A., Snider, N.O., 2001. Repeating deep earthquakes: evidence for fault reactivation at great depth. Science 293 (5534), 1463–1466.
Wiens, D.A., McGuire, J.J., Shore, P.J., 1993. Evidence for transformational faulting from a deep double seismic zone in Tonga. Nature 364 (6440), 790–793.

Xi, Z., Wei, S.S., Zhu, W., Beroza, G.C., Jie, Y., Saloor, N., 2024. Deep learning for deep earthquakes: insights from OBS observations of the Tonga Subduction Zone. Geophys. J. Int. 238 (2), 1073–1088 (p.ggae200).
Xu, W., Peng, X., Stern, R.J., Xu, X., Xu, H., 2023. Challenger deep basalts reveal Indian-type Early Cretaceous oceanic crust subducting in the southernmost Mariana Trench. Geology 51 (9), 865–869.
Yamasaki, T., Seno, T., 2003. Double seismic zone and dehydration embrittlement of the subducting slab. J. Geophys. Res. 108 (B4).
Zeng, L., Ye, L., Yao, H., Liu, W., Si, D., Lay, T., Yang, T., 2025. Narrow intermediate-depth seismogenic band related to flexural strain in relatively dry Peruvian flat slab. Commun. Earth Environ. 6 (1), 104.
Zhan, Z., 2020. Mechanisms and implications of deep earthquakes. Annu. Rev. Earth Planet. Sci. 48, 147–174.
Zhang, M., Ellsworth, W.L., Beroza, G.C., 2019. Rapid earthquake association and location. Seismol. Res. Lett. 90 (6), 2276–2284.
Zhang, Z., Dong, D., Sun, W., Zhang, G., 2021. The Caroline Ridge fault system and implications for the bending-related faulting of incoming oceanic plateaus. Gondw. Res. 92, 133–148.
Zhang, J., Zhang, F., Yang, H., Lin, J., Sun, Z., 2022. The effects of plateau subduction on plate bending, stress and intraplate seismicity. Terra Nova 34 (2), 113–122.
Zhang, J., Zhang, G., Jonny, W., 2023a. Geochemical and geochronological constraints on the tectonic and magmatic evolution of the southwestern Mariana subduction zone. Deep Sea Res. I 197, 104039.
Zhang, X., Brown, E.L., Zhang, J., Lin, J., Bao, X., Sager, W.W., 2023b. Magmatism of Shatsky Rise controlled by plume–ridge interaction. Nat. Geosci. 16 (11), 1061–1069.
Zhao, D., Xu, Y., Wiens, D.A., Dorman, L., Hildebrand, J., Webb, S., 1997. Depth extent of the Lau back-arc spreading center and its relation to subduction processes. Science 278 (5336), 254–257.
Zhong, Y., Zhang, J., Li, S., Zhang, G.L., 2025. A young crustal component in the Caroline mantle plume (Western Pacific Ocean). Geophys. Res. Lett. 52 (13) (e2024GL114031).
Zhou, Z., Lin, J., 2018. Elasto-plastic deformation and plate weakening due to normal faulting in the subducting plate along the Mariana Trench. Tectonophysics 734-735, 59–68.
Zhou, Z., Lin, J., Behn, M.D., Olive, J.-A., 2015. Mechanism for normal faulting in the subducting plate at the Mariana Trench. Geophys. Res. Lett. 42 (11), 4309–4317.
Zhu, G., Yang, H., Lin, J., Zhou, Z., Xu, M., Sun, J., Wan, K., 2019. Along-strike variation in slab geometry at the southern Mariana subduction zone revealed by seismicity through ocean bottom seismic experiments. Geophys. J. Int. 218 (3), 2122–2135.
Zhu, H., Li, X., Yang, J., Stern, R.J., Lumley, D.E., 2020. Poloidal- and Toroidal-Mode Mantle flows underneath the Cascadia Subduction Zone. Geophys. Res. Lett. 47 (14) (p. e2020GL087530).
Zhu, G., Wiens, D.A., Yang, H., Lin, J., Xu, M., You, Q., 2021. Upper mantle hydration indicated by decreased shear velocity near the Southern Mariana Trench from Rayleigh wave tomography. Geophys. Res. Lett. 48 (15) (p. e2021GL093309).
Zhu, G., Yang, H., Gao, X., Dong, D., Fan, J., Zhang, G., Li, C., 2024. A steep slab at the Yap Trench resulted from subducting oceanic plateaus. Seismol. Res. Lett. 96, 473–483. https://doi.org/10.1785/0220240051.